Bioconjugation of holo-transferrin with hypoxia-enhanced fluorescent sensor for the selective imaging of cancer cells

Ewelina Janczy-Cempa [a], Anna Kwiatkowska [a,b], Olga Mazuryk [a], Nicolas Chopin [b], Marie-Aude Hiebel [b], Franck Suzenet [b,*], Malgorzata Brindell [a,*]

[a] *Department of Inorganic Chemistry, Faculty of Chemistry, Jagiellonian University in Krakow, Gronostajowa 2, Kraków 30-387, Poland*
[b] *Institute of Organic and Analytical Chemistry, University of Orléans, UMR-CNRS 7311, rue de Chartres, BP 6759, Orléans Cedex 2 45067, France*

A R T I C L E I N F O

A B S T R A C T

A new fluorescent sensor for imaging cancer cells was designed by bioconjugation of holo-transferrin (hTf) with a nitro-pyrazinotriazapentalene moiety (**PyTAP-NO$_2$**) as a bioreductive fluorescent unit. hTf was chosen to increase its selective delivery to cancer cells through transferrin receptor (TfR) mediated endocytosis. **PyTAP-NO$_2$** was applied to enhance the fluorescent signal in oxygen-deprived cells due to the increased expression of nitroreductases under such conditions. A protein-dye bioconjugate had an average of 8 fluorophore molecules per protein that effectively amplifying the fluorescence signal. The designed **hTf- PyTAP-NO$_2$** was non-toxic and its efficient accumulation through TfR, as well as its high stability and sustained intracellular retention, was proven. **hTf-PyTAP-NO$_2$** bioconjugate allows selective accumulation in cancer cells containing increased levels of TfRs with simultaneous slight enhancement of signal in hypoxic cells due to increased expression of nitroreductases.

1. Introduction

Imaging cancer cells is of great importance not only for locating them within the whole body but also for determining their development stage, following the effectiveness of treatment, and finally for providing detailed information that can be used while performing surgery [1]. Surgical cancer removal is one of the most effective treatments; however, a complete resection of malignant tissue with adequate tumor-free margins is critical. To help in the recognition of the margin extent of the tumor front and subsequently the adequacy of the excision of the primary tumor, a real-time imaging technique is needed. Among others, fluorescence-based visualization methods due to their superior sensitivity, resolution, and high safety can provide real-time feedback for the delineation of tumors during surgery and recently the resulting medical procedures have attracted the attention of scientists [2,3]. To use fluorescence imaging for the visualization of cancer, tumor-specific fluorescent agents are necessary. They can be designed based on cancer

hallmarks [4,5]. The first-in-human study on intraoperative tumor-specific fluorescence imaging were already successfully conducted applying, among others, folate and fluoresceine isothiocyanate conjugate ($\lambda_{ex/em}$ 490/525 nm) or bevacizumab conjugated to IRDye800CW dye ($\lambda_{ex/em}$ NIR) [6–8].

In one of the approaches to achieve target-specific fluorescence imaging, fluorescent agents can be delivered to tumor cells using transferrin (Tf) as a natural carrier. Tf is a plasma glycoprotein with a primary function of serum iron transportation. It reversibly binds two atoms of ferric iron (Fe^{3+}) with high affinity (10^{-22} M^{-1}, at pH 7.4), and differic transferrin is called holo-transferrin (hTf) [9]. Neoplastic cells due to abnormal proliferation and increased DNA synthesis show an increased need for iron compared to healthy cells [10]. To meet these requirements, cancer cells overexpress a panel of proteins involved in iron metabolism, especially the transferrin receptor (TfR), responsible for delivering iron inside the cell by binding hTf, and its internalization via receptor-mediated endocytosis into the endosome [11,12]. Acidification

Scheme 1. The mechanism of reduction of nitroaromatic compound by type-I and -II nitroreductases (adapted from [32,33]).

inside the endosome leads to the release of iron and its further transport to the cytoplasm by the DMT1 iron transporter, while remaining apo-transferrin (aTf) and TfR are recycled back to the extracellular environment [13]. hTf has 10- to 100-fold higher affinity for TfR compared to aTf under physiological conditions [14]. TfR is expressed in neoplastic cells at a level that is many times higher than in normal cells, and its expression is correlated with the stage of cancer and its progression. For these reasons, TfR is an attractive target for diagnosis and therapy [15,16]. Its natural ligand, hTf, is selected for conjugating drugs or diagnostic compounds, improving their internalization and selectivity for delivery to tumor tissue while minimizing side effects [17,18]. One should pay attention to the fact that approximately 85–95 % of the TfR-transferrin complex follows the recycling pathway, which brings them back to the cell surface [13]. Therefore, the cargo (drug or sensor) needs to be effectively released or modified transferrin needs to be trapped inside the cell.
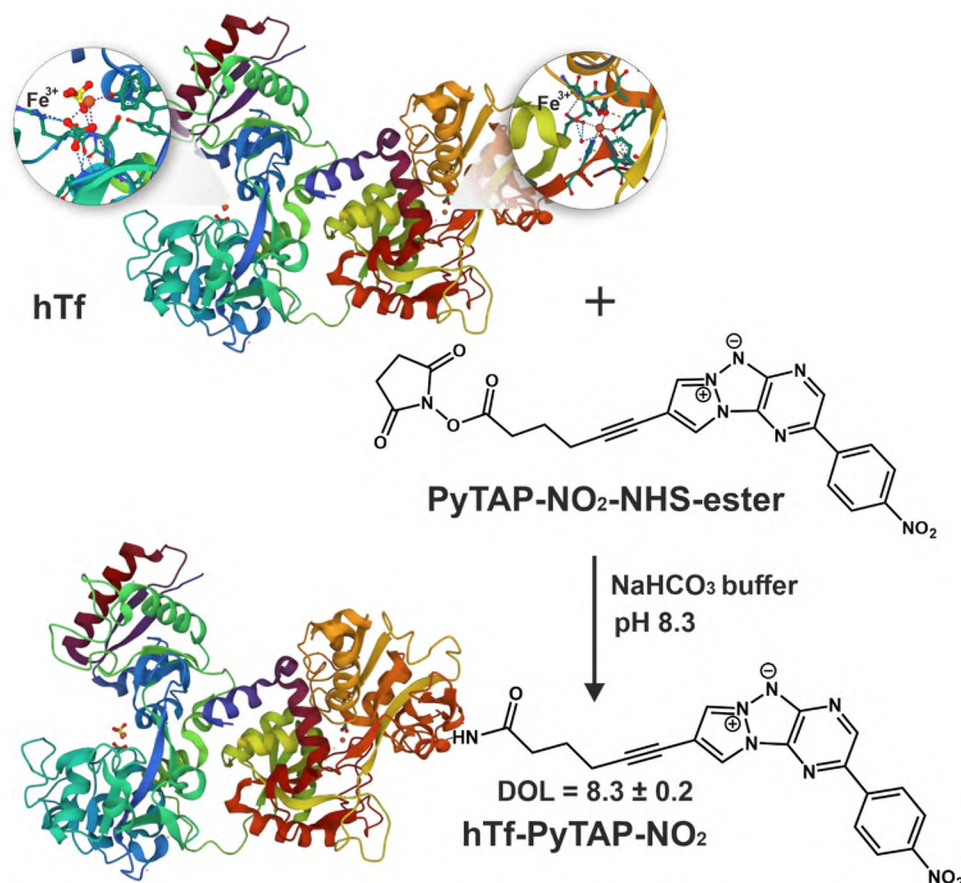

Fig. 1. Reaction pathway for the conjugation of **PyTAP-NO$_2$** sensor with holo-transferrin (hTf). For clarity the conjugation of one sensor molecule is shown in the scheme, however, the average number of fluorophore molecules per molecule of hTf (degree of labeling, DOL) was ca. 8.

Furthermore, one of the crucial microenvironmental features in most solid tumors is the chronically lowered level of oxygen in cancer tissue (< 5–10 mmHg) called hypoxia [19]. Areas of hypoxia in tumor tissues result from a limited oxygen supply due to inefficient blood vessel formation in rapidly growing tumor tissues. The occurrence of chronic hypoxia in cancer tumors induces the activation of complex intracellular signaling pathways necessary for cellular adaptation to hypoxia stress. One of the most crucial responses is the overexpression of the oxygen-sensitive transcription factor HIF-1 (hypoxia-inducible factor 1), which activates more than 30 genes involved in various cellular pathways [20–22]. The hypoxic state usually promotes increased genetic instability and aggressiveness of the cancer cell phenotype. That leads to a poorer efficacy of anticancer therapies (chemotherapy, radiotherapy, or photodynamic therapy) and a poor prognosis [23]. Due to severe negative effects, it is very important to detect hypoxic cells during imaging. However, the delivery of fluorescent agents for imaging is usually hampered by the lack of adequate vascularization. To overcome this problem, a TfR-mediated delivery system can be applied, since its activity is regulated, among others, by hypoxia, which induces the transcription of the TFR1 gene [24]. Additionally, fluorophores whose emission can be enhanced in a hypoxic environment may have an additional advantage.

One common adaptive mechanism of hypoxic tumor cells is an increase in the contribution of glycolysis to metabolism, resulting in a change in the redox potential and a more reductive environment, compared to normal tissues. These microenvironmental conditions favor the overexpression of many redox enzymes, such as oxidoreductases [25–27]. Among them are nitroreductases (NTRs) that catalyze the reduction of nitroaromatic compounds in the presence of NAD(P)H as the reducing agent and flavin mononucleotide (FMN) or flavin adenine dinucleotide (FAD) as the prosthetic group [28–30]. In type I NTRs first step is the oxygen-independent two-electron reduction, while in type II NTRs oxygen-sensitive one-electron reduction functions only in extreme hypoxia environments [31]. The subsequent reaction steps are shown in Scheme 1 along with examples of Type I and II NTRs.

One of the approaches in designing fluorescent agents for imaging cancer cells is to take advantage of the increased expression or activity of NTRs [12,32,34–36]. Small molecular sensors consist of a fluorophore, a linker, and a nitroaromatic moiety that quenches the fluorescence of fluorophore and is also a substrate for nitroreductases [37–40]. NTRs can convert non-fluorescent or weakly fluorescent compounds into fluorescent ones through irreversible reduction of the nitro group shown in Scheme 1, allowing them to be used for imaging hypoxic cancer cells [41–43]. Recently our group has designed fluorescent sensors based on pyrazine-1,3a,6a-triazapentalene fluorophore coupled with a hypoxia-sensitive nitrophenyl moiety that in the presence of NTRs underwent irreversible reduction to a highly fluorescent form [33]. These probes exhibited high sensitivity towards NTRs with a detection limit as low as 20–30 ng/mL. *In vitro* studies on A2058 melanoma cells showed their low toxicity, high photostability efficient uptake, and enhanced imaging properties under hypoxic conditions.

Considering the requirements for imaging cancer cells described above and based on our previous experience, we have designed a new fluorescent sensor by bioconjugation of hTf with a nitro-pyrazinotriazapentalene scaffold (Fig. 1). The aim of such a combination was to increase its selective delivery to cancer cells by exploiting TfR and enhancing the fluorescent signal in hypoxic cells due to the increased expression of NTRs. Holo-transferrin was chosen because of its high affinity for TfR. N-hydroxysuccinimide ester was employed as the dynamic covalent linker to prepare a multifunctional protein-dye bioconjugate to effectively increase the number of hypoxia-sensitive units. We report here the synthetic pathways for obtaining the dye and its bioconjugation to hTf and bioconjugate response to NTRs. *In vitro* studies are focused on the evaluation of the imaging properties of the bioconjugate along with the demonstration of its uptake via the TfR-mediated endocytosis, enhanced fluorescent signal under hypoxia, and

high retention in cells.

2. Material and methods

2.1. Synthesis and characterization of PyTAP-NO2-NHS-ester dye

2.1.1. General chemistry

Unless otherwise specified, all reagent-grade chemicals and solvents - commercially available, were used without further purification. ^{1}H and ^{13}C NMR spectra were recorded on the Bruker Avance DPX-250 (250 MHz) and Bruker Avance 400 (400 MHz) spectrometers, reporting chemical shifts (δ) in ppm and coupling constants (J) in Hz. Chemical shifts were analyzed in reference to the solvent peaks (DMSO-d6, CDCl$_3$).

High-resolution mass spectra (HRMS) were registered on a Bruker maXis mass spectrometer by the "Fédération de Recherche" ICOA/CBM (FR2708) platform. Low-resolution mass spectra were recorded on a Thermo Scientific Endura mass spectrometer. Thin-layer chromatography (TLC) was performed with the use of aluminum sheets pre-coated Silica Gel 60 F254 (Merck), which were visualized with ultraviolet light at 254 nm. Purification of compounds included the column chromatography on Silica Gel 60 (230 − 400 mesh, Merck). Melting points were determined using Thermo Scientific 9200 apparatus with capillary tubes. The infrared spectra were recorded on a Thermo Scientific Nicolet iS10 FT-IR and maximum absorption wavenumbers v'' are given in cm^{-1}. Experimental details for the photophysical characterization (absorption and emission spectra, the quantum yield of luminescence (Φ), are described in paragraph 2).

Additionally, the synthesis of the substrate **1** is presented in the in paragraph 8. Preparation of PyTAP is precisely described in M. Daniel et al. [44].

2.1.2. Methyl 6-(1-(3-amino-6-bromopyrazin-2-yl) − 1 H-pyrazol-4-yl) hex-5-ynoate (2)

In a round bottom flask, 2-amino-5-bromo-3-chloropyrazine [33] (100 mg, 0.48 mmol), **1** (134 mg, 0.72 mmol) and Cs$_2$CO$_3$ (234 mg, 0.72 mmol) were dissolved in dry DMF under argon atmosphere. The mixture was heated at 70 °C for 3 h. At the end of the reaction, water was added, and the resulting mixture was extracted with ethyl acetate. The combined organic phase was washed with water, dried with MgSO$_4$ and concentrated under reduced pressure. The crude product was purified by column chromatography on silica gel (eluent DCM/AcOEt 9/1) to obtain the desired compound **2** as a pale-yellow solid (151.1 mg, 87 %). mp: 109 °C. ^{1}H NMR (400 MHz, CDCl$_3$) δ 8.56 (s, 1 H), 8.00 (s, 1 H), 7.71 (s, 1 H), 6.60 (s, 2 H), 3.69 (s, 3 H), 2.49 (q, $J = 7.9$ Hz, 4 H), 1.92 (qu, $J = 7.2$ Hz, 2 H). ^{13}C NMR (101 MHz, CDCl$_3$) δ 173.7, 145.3, 143.4, 141.8, 131.5, 130.9, 121.5, 106.2, 91.8, 71.3, 51.8, 33.0, 23.9, 19.1. IR (cm^{-1}) v 3403, 3267, 3158, 2954, 1728, 1608, 1469, 1453, 1425, 1378, 1354, 1332, 1258, 1219, 1198, 1172, 1145, 1023, 963, 876, 847. HRMS (ESI) m/z: calculated for C$_{14}$H$_{15}^{79}$BrN$_5$O$_2$ [M + H]$^+$ 364.040363; found 364.040241.

2.1.3. Methyl 6-(1-(3-amino-6-(4-nitrophenyl)pyrazin-2-yl) − 1 H-pyrazol-4-yl)hex-5-ynoate (3)

In a sealed tube, **2** (100 mg, 0.28 mmol) was introduced with para-nitrophenylboronic acid (70 mg, 0.42 mmol), Pd(PPh$_3$)$_4$ (16 mg, 0.014 mol) and K$_2$CO$_3$ (77 mg, 0.56 mmol) under argon atmosphere. The solids were dissolved in methanol (4 mL) and the mixture was heated at 100 °C for 3 h. After concentration under reduced pressure, the crude product was purified by column chromatography on silica gel (eluent DCM/AcOEt 9/1) to obtain the desired compound **3** as a yellow solid (95 mg, 83 %). mp 175 °C. ^{1}H NMR (400 MHz, CDCl$_3$) δ 8.71 (s, 1 H), 8.49 (s, 1 H), 8.29 (d, $J = 8.5$ Hz, 2 H), 8.07 (d, $J = 8.5$ Hz, 2 H), 7.76 (s, 1 H), 6.89 (s, 2 H), 3.70 (s, 3 H), 2.52 (q, $J = 7.5$ Hz, 4 H), 1.95 (qu, $J = 7.2$ Hz, 2 H). ^{13}C NMR (101 MHz, CDCl$_3$) δ 173.7, 147.5, 146.3, 143.3, 142.3, 138.0, 135.9, 131.7, 130.5, 125.8, 124.4, 106.1, 91.9,

71.4, 51.8, 33.1, 24.0, 19.1. IR (cm^{-1}) ν 3380, 3267, 3126, 2950, 1731, 1620, 1593, 1532, 1510, 1480, 1435, 1404, 1337, 1248, 1215, 1178, 1111, 1052, 1022, 963, 851. HRMS (ESI) m/z: calculated for $C_{20}H_{19}N_6O_4$ [M + H]$^+$ 407.146230; found 407.146209.

2.1.4. 8-(6-Methoxy-6-oxohex-1-yn-1-yl) − 2-(4-nitrophenyl)pyrazolo [1',2':1,2][1–3]triazolo-[4,5-b]pyrazin-6-ium-5-ide (4)

In round bottom flask, **3** (216 mg, 0.53 mmol,) was dissolved in degassed DMSO (4 mL) under argon atmosphere. NaH 60 % dispersion in mineral oil (53 mg, 1.33 mmol) was added to the mixture and stirred for 10 min before adding PhI(OAc)$_2$ (341 mg, 1.06 mmol). The mixture was heated at 80 °C for 1 h then cooled to room temperature and filtrated over Celite. The crude product was purified by column chromatography on silica gel (eluent DCM/AcOEt 9/1) to obtain the desired compound **4** as a red solid (46 mg, 22 %). mp: 143 °C. ^{1}H NMR (400 MHz, CDCl$_3$) δ 8.98 (s, 1 H), 8.30 (d, $J = 8.5$ Hz, 2 H), 8.18 – 8.12 (m, 3 H), 7.87 (s, 1 H), 3.70 (s, 3 H), 2.57 – 2.47 (m, 4 H), 1.96 (qt, $J = 7.2$ Hz, 2 H). ^{13}C NMR (101 MHz, CDCl$_3$) δ 173.4, 152.5, 147.5, 142.8, 141.8, 136.7, 129.0, 127.0, 126.4, 124.4, 113.0, 112.1, 108.5, 94.0, 70.0, 51.8, 33.0, 23.6, 19.0. IR (cm^{-1}) ν 3113, 2952, 1729, 1581, 1511, 1435, 1339, 1203, 1108, 853, 752, 691, 601. HRMS (ESI) m/z: calculated for $C_{20}H_{17}N_6O_4$ [M + H]$^+$ 405.130579; found 405.130776.

2.1.5. Synthesis of the PyTAP-NO2-NHS ester

In a round bottom flask, **4** (188 mg, 0.47 mmol) was dissolved in MeOH (3.2 mL) and NaOH 1 M (10 mL) was added in 4 portions (ca. 2.5 mL per h). After complete conversion, the reaction mixture was neutralized then extracted with DCM and washed with water. The organic phase was dried with MgSO$_4$ and concentrated under reduced pressure. The residue was dissolved in DCM (4 mL). N-hydroxysuccinimide and (60 mg, 0.52 mmol) and 1-ethyl-3-(3-dimethylaminopropyl)carbodiimide (81 mg, 0.52 mmol) were added to the mixture which was stirred at room temperature for 3 h. At the end of the reaction, water was added, and the resulting mixture was extracted with DCM. The combined organic phase was washed with water, dried with MgSO$_4$ and concentrated under reduced pressure. The crude product was purified by column chromatography on silica gel (eluent DCM/AcOEt 1/1) to obtain the desired **PyTAP-NO$_2$-NHS ester** as a red solid (41 mg, 18 %). mp: 226 °C (degradation). ^{1}H NMR (400 MHz, DMSO-*d6*) δ 9.22 (d, $J = 1.6$ Hz, 1 H), 9.06 (s, 1 H), 8.77 (s, 1 H), 8.36 (t, $J = 1.8$ Hz, 4 H), 2.94–2.86 (m, 2 H), 2.85 (bs, 4 H), 2.65 (t, $J = 7.2$ Hz, 2 H), 2.05 – 1.90 (m, 2 H). ^{13}C NMR (101 MHz, DMSO-*d6*) δ 170.2, 168.6, 152.0, 146.6, 142.9, 141.5, 134.5, 129.2, 126.0, 124.2, 115.4, 113.2, 106.9, 92.6, 71.0, 29.4, 25.5, 23.4, 17.8. IR (cm^{-1}) ν 3134, 2937, 1808, 1781, 1733, 1578, 1513, 1492, 1438, 1386, 1339, 1318, 1201, 1092, 1066, 991, 905, 854, 789, 766, 751, 691, 646, 602. HRMS (ESI) m/z: calculated for $C_{23}H_{18}N_7O_6$ [M + H]$^+$ 488.131308; found 488.130720.

2.2. Bioconjugation of PyTAP-NO$_2$-NHS-ester to hTf

To a solution of hTf (75 µM) in 0.1 M sodium bicarbonate buffer pH 8.3 a ten-fold molar excess of **PyTAP-NO$_2$-NHS ester** (750 µM) dissolved in anhydrous DMSO was added. The final concentration of DMSO in the solution was fixed at 5 % (v/v). The reaction mixture was gently stirred for 1.5 h at RT in the dark. To stop the reaction, hydroxylamine (0.15 M, pH 8.5 in water) was added to the solution and incubated for 1 h. Subsequently, the conjugated protein was purified from the unreacted dye by ultrafiltration (cut-off 30 kDa, Amicon), and the protein bioconjugate was characterized by absorption spectroscopy and stored at − 20 °C in aliquots. To calculate the degree of labeling (DOL), the protein concentration was determined using the Bradford Protein Assay, and the number of ligands (**PyTAP-NO$_2$**) linked to hTf were calculated using the absorption coefficient for **PyTAP-NO$_2$-NHS-ester** (ε at 450 nm 19000 mol$^{-1} \cdot$cm^{-1}). DOL was determined from measurements for three independently prepared bioconjugates.

2.3. Reduction of the bioconjugate by type I nitroreductase

Nitroreductase, NTR, from Escherichia coli (Sigma-Aldrich N9284) was used to check the reduction of nitro groups in the **hTf-PyTAP-NO$_2$** bioconjugate by type I NTRs. The reduction was monitored by following changes in the emission spectra (from 480 to 800 nm) of the bioconjugate upon excitation at 450 nm using a spectrofluorometer (Perkin Elmer L55) while the absorption spectra were recorded on a Perkin Elmer Lambda 35 spectrophotometer. Typical conditions involved 3.3 µM of **hTf-PyTAP-NO$_2$** (which corresponds to 28 µM of the nitro group in the bioconjugate), 400 µM NADH, and 4.8 µg/mL of NTR. For checking the concentration dependence fluorescence spectra were measured with different NTR concentrations up to 30 µg/mL. The reaction was conducted in 50 mM TRIS-HCl buffer pH 7.4 at 37 °C. Before each measurement, the tested solutions were incubated for 5 min at 37 °C, followed by the addition of the enzyme. A blank solution with **hTf-PyTAP-NO$_2$** and NADH in the absence of NTR was also prepared and measured under the same conditions.

2.4. Reduction of the bioconjugate by type II nitroreductase

Rat liver microsomes (Sigma-Aldrich M9066) were used as a source of type II NTRs. Typical reduction conditions involved 3.3 µM **hTf-PyTAP-NO$_2$**, 1 mM NADH and 1 mg/mL of liver microsomes, and the reaction was carried out in 50 mM TRIS-HCl buffer pH 7.4 at 37 °C for 6 h. The reaction was carried out under air-equilibrated conditions and in a glovebox (Inert, I-Lab) with a pO$_2$ content below 1 ppm. The progress of the reduction and was determined using a plate reader (Tecan Infinite 200) by monitoring emission spectra in the range 480–750 nm upon excitation at 450 nm.

2.5. Cell culturing

In vitro studies were conducted using the human highly metastatic melanoma A2058 cell line. Cells were cultured in EMEM medium supplemented with 2 mM glutamine, 1 % non-essential amino acids (NEAA) (v/v), 10 % fetal bovine serum (FBS) (v/v) and 1 % penicillin-streptomycin solution (100 units/mL-100 µg/mL) (v/v). Cells were routinely cultured at 37 °C in a humidified incubator in a 5 % CO$_2$ atmosphere. Hypoxic conditions were maintained in a humidified hypoxic chamber (Coy) filled with a gas mixture comprising of 94 % N$_2$, 5 % CO$_2$, and 1 % O$_2$. For hypoxia screens, cells were seeded under normal conditions and after 2 – 4 h of incubation moved to the hypoxic chamber for at least 24 h preincubation. The medium intended to be used in hypoxic experiments was also preincubated in the hypoxic chamber for at least 24 h. Experimental details of the evaluation of **hTf-PyTAP-NO$_2$** cytotoxicity and photocytotoxicity are in paragraph 5.

2.6. Uptake of the bioconjugate

A2058 cells were seeded into a 96-well plate with a density of 3×10^4 cells per cm^2 in a complete medium and cultured for 24 h. Subsequently, the medium was removed, and cells were treated with various concentrations of the **hTf-PyTAP-NO$_2$** in a basic medium supplemented with 20 mM glucose for a period (1 – 24 h) in normoxic conditions. Afterwards, cells were washed with PBS, and the fluorescence at 530 nm upon excitation at 450 nm was measured using a microplate reader (Tecan Infinite 200). Experiments were performed in triplicates and repeated three times. Results are presented as mean values and standard error of the mean.

2.7. Bioimaging of cells

A2058 cells were seeded into a 96-well plate with a density of 3×10^4 cells per cm^2 and cultured for 24 h in complete medium under normoxic (21 % O$_2$) or hypoxic conditions (1 % O$_2$). Next, (still under
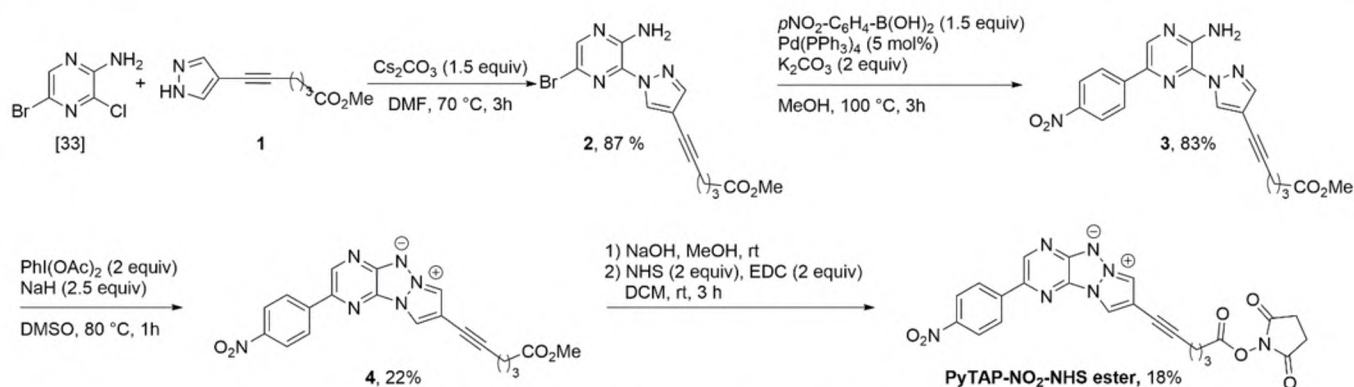
Scheme 2. Synthetic pathway to **PyTAP-NO₂-NHS-ester**.

hypoxic or normoxic conditions) various concentrations of the **hTf-PyTAP-NO₂** were added and incubated for a different period. Subsequently, the incubated cells were washed with PBS and fluorescent images were taken using an Olympus IX83 microscope equipped with a CellVivo chamber (λ_{ext} (470 ± 20) nm, λ_{em} (525 ± 25) nm).

2.7.1. Quantification of fluorescence intensity in cell suspension by flow cytometry

A2058 cells were seeded into a 6-well plate with a density of 1.5×10^4 cells per cm^2 in a complete medium and cultured for 24 h in normoxia (21 % O₂) or hypoxia (1 % O₂). Then the complete medium was removed, and the cells were incubated with **hTf-PyTAP-NO₂** (0.6 μM or 1.2 μM) in a basic medium supplemented with 20 mM glucose for 2 or 4 h. Next, cells were washed with PBS buffer, and after detachment by trypsin, the cells were suspended in PBS buffer and analyzed using a BD FACS Verse cytometer applying different channels FITC (488/527 ± 16 nm), PE (488/586 ± 21 nm), and PerCP (488/700 ± 27 nm). The experiment was performed three times and the mean values and standard error of the mean are presented.

2.8. Sensor retention in cells

To evaluate the removal of dye (in the form of bioconjugate with transferrin or alone) from cells, A2058 cells were seeded into a 6-well plate with a density of 1.5×10^4 cells per cm^2 in a complete medium and cultured for 24 h in normoxia (21 % O₂) or hypoxia (1 % O₂). Then, the complete medium was removed, and the cells were incubated with **hTf-PyTAP-NO₂** (0.6 μM or 1.2 μM) in a basic medium supplemented with 20 mM glucose for 4 h. The cells were then washed with PBS buffer and left in a new batch of buffer for a specified period after removal of the sensor (0, 2, 4, 6 or 24 h). After this time, the PBS was collected from the cells and the cells were detached by trypsinization, suspended in PBS buffer, and analyzed using a BD FACS Verse cytometer (FITC channel 488 nm/527 nm ± 16 nm). The experiment was performed three times and the mean values, and the standard error of the mean were presented.

2.9. Inhibition of transferrin receptor-mediated uptake of the bioconjugate

To evaluate the impact of transferrin receptor-mediated uptake on the accumulation of **hTf-PyTAP-NO₂** in cells, A2058 cells were seeded into 96-well plates with a density of 3×10^4 cells per cm^2 in a complete medium and cultured for 24 h. Then, 100 μM ferristatin II (Chlorazol Black, Merck) – a TfR1 inhibitor – dissolved in the basal medium supplemented with 20 mM glucose was added for another 24 h of incubation. Next, the medium was removed and either commercially available Tf-AlexaFluor488 bioconjugate (Thermo Fisher Scientific, 0.6 or 1.2 μM) and **hTf-PyTAP-NO₂** bioconjugate (2 or 4 μM) were added and incubated for 4 h in a basic medium supplemented with 20 mM glucose and 100 μM ferristatin II. Similarly, both probes were added to cells not

preincubated with ferristatin II. Subsequently, the incubated cells were washed with PBS and fluorescent images were taken using an Olympus IX83 microscope equipped with a CellVivo chamber (λ_{ex} (470 ± 20) nm, λ_{em} (525 ± 25) nm). Untreated cells were used as a control.

In a competitive experiment, A2058 cells prepared in the same way as for imaging experiment were treated with **hTf-PyTAP-NO₂** (0.6 or 1.2 μM) alone or in the presence of a10-fold excess of hTf (6 or 12 μM). Cells preincubated with ferristatin II were also treated with **hTf-PyTAP-NO₂** (0.6 or 1.2 μM). After 1 h of incubation, cells were washed with PBS and the fluorescence intensity of the cells was quantified at 530 nm after excitation at 450 nm using a microplate reader (Tecan Infinite 200). Untreated cells were used as a control.

3. Results and discussion

3.1. Synthesis and characterization of PyTAP-NO2-NHS-ester dye and its conjugation to hTf

The fluorescent properties of pyrazino-1,3a,6a-triazapentalene (**PyTAP**) derivatives were recently reported [45,46] and their synthesis can be achieved through three main synthetic pathways: deoxygenation from nitro derivatives [47] thermolysis from azide derivatives[45] or oxidative cyclisation from amine derivatives [44]. With respect to nitro-containing probes, the amine approach was used. The synthesis started with a S$_N$Ar reaction between 2-amino-5-bromo-4-chloropyrazine [44] and pyrazole **1** (see SI section for more details). Then, a Suzuki-Miyaura cross coupling reaction occurs in the presence of palladium tetrakis triphenylphosphine with p-nitrophenylboronic acid leading to **3** with an excellent yield. Due to the favorable electron-withdrawing character of the nitrophenyl group, the key N-N bond formation was carried out in the presence of PhI(OAc)₂ and NaH in DMSO to afford the pyrazinotriazapentalene **4** in a moderate yield. Finally, the ester group was hydrolyzed under basic conditions and the carboxylic acid group of the dye was converted into an activated ester using N-hydroxysuccinimide (NHS) and 1-ethyl-3-(3-dimethylamino-propyl)carbodiimide (EDC) yielding the desired **PyTAP--NO₂-NHS-ester** with 18 % efficiency over the two steps. The reaction steps are shown in Scheme 2. The photophysical data for the synthesized compound and data for **PyTAP** as reference (i.e., unsubstituted pyridazino-1,3a,6a-triazapentalene) are collected in Table S1.

The preparation of the transferrin-based bioconjugate **hTf-PyTAP-NO₂** is shown schematically in Fig. 1. **PyTAP-NO₂-NHS-ester** (10-fold excess) was conjugated to hTf via a reaction of the NHS ester group with the amino group of the lysine residues present in hTf. After performing the conjugation, an aqueous solution of hydroxylamine was added to the reaction mixture to interact with the NHS ester group of the unreacted probe, preventing any further reaction. The efficiency of the conjugation and purification by ultrafiltration of the formed adducts were evaluated by applying fast protein liquid chromatography (FPLC) with an anion
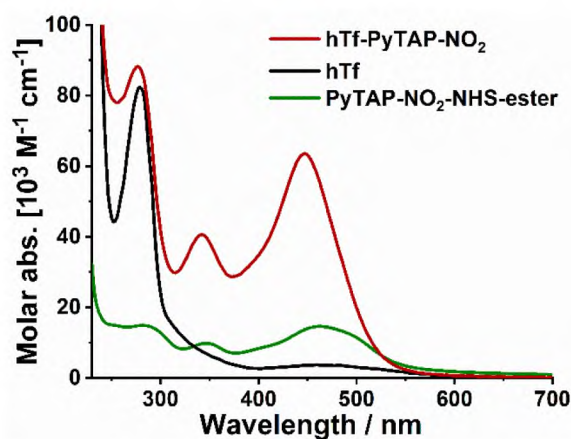
Fig. 2. Absorption spectra of holo-transferrin (hTf, black), **PyTAP-NO₂-NHS-ester** (green) and **hTf-PyTAP-NO₂** bioconjugate (red) in water.
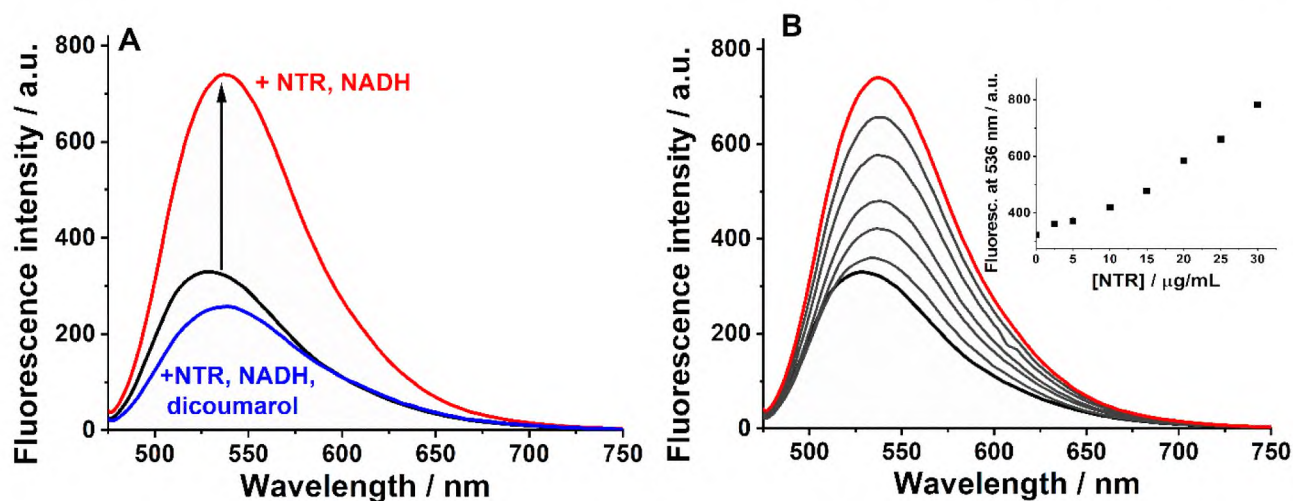
exchange column. FPLC analysis of the **hTf-PyTAP-NO₂** bioconjugates showed an almost complete absence of the native transferrin and the free dye (Fig. S1). Tf possesses 58 lysine residues, so it is expected that more than one of the amino groups is conjugated to the probe leading to a mixture of modified transferrin with various degree of labeling (DOL). The calculated DOL specifying the average number of fluorophore molecules per molecule of bioconjugate and was 8.3 ± 0.2.

The UV-Vis absorption spectra (Fig. 2) also confirm that in the **hTf-PyTAP-NO₂** bioconjugate, several dyes are attached to the hTf. A hypsochromic shift in the absorption band from 464 to 447 nm compared to the free **PyTAP-NO₂-NHS-ester** was observed.

3.2. Response of hTf-PyTAP-NO2 bioconjugate to type I nitroreductase

To examine the response of the tested sensor to nitroreductases that might be overexpressed in hypoxic tumor cells, type I oxygen-insensitive nitroreductase (NTR type I), from *Escherichia coli* encoded by the NfsB gene was used. In previous studies it was shown that the nitro-pyrazinotriazapentalene derivatives are characterized by a very low fluorescence at 541 nm in DMSO due to the effective quenching of the

Fig. 3. **A)** Fluorescence emission spectra of **hTf-PyTAP-NO₂** (3.3 μM) before (black line), and after the addition of nitroreductase, NTR (30 μg/mL) in the presence of NADH after 1 h incubation in the absence (red line) or the presence of 200 μM dicoumarol (blue line). **B)** Fluorescence emission spectral changes of **hTf-PyTAP-NO₂** (3.3 μM) in the presence of various concentrations of NTR (2.5–30 μg/mL). *Inset*: A correlation between fluorescence intensities at 536 nm and concentrations of NTR after incubation with **hTf-PyTAP-NO₂**. Reaction conditions: 400 μM NADH, TRIS-HCl buffer (pH 7.4, 50 mM), 37 °C, air-equilibrated conditions, λ_{ex} 450 nm.
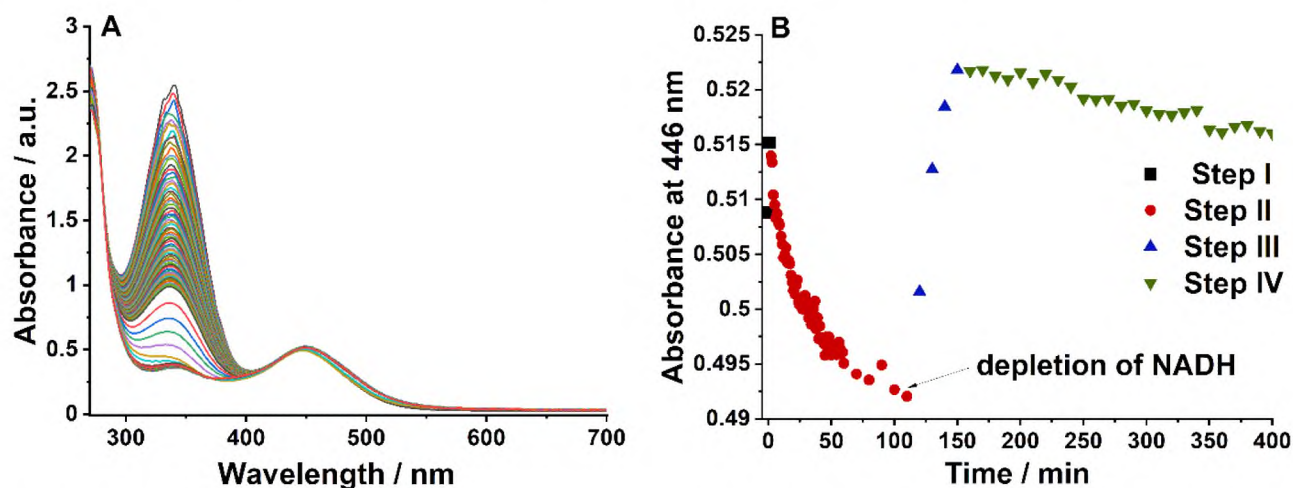

Fig. 4. Time-dependent changes in absorption spectrum (**A**) or absorbance at the selected wavelength (**B**) for **hTf-PyTAP-NO₂** (3.3 μM) in the presence of 400 μM NADH and NTR (30 μg/mL) recorded at 37 °C, TRIS-HCl buffer (pH 7.4, 50 mM).

fluorophore by the nitroaromatic group, while after the reduction by NTR they are converted into strongly emissive compounds [33]. In contrast, the obtained **hTf-PyTAP-NO$_2$** bioconjugate already exhibited fluorescence at 530 nm after excitation at 450 nm (Fig. 3A). This increase of the fluorescence intensity combined with the blue shift for the emission wavelength are consistent with the positive solvatochromism of PyTAP derivatives. One can assume that the nitro-pyrazinotriazapentalene scaffold binds in a hydrophobic environment of the hTf protein that prevents fluorescence quenching by water molecules. Importantly, the intensity of fluorescence of **hTf-PyTAP-NO$_2$** bioconjugate is distinctly increased upon the addition of NTR in the presence of NADH and the maximum is shifted to 537 nm (Fig. 3A). Such an increase is suppressed upon the addition of dicoumarol (Fig. 3A), a competitive inhibitor of NADH, confirming that the observed response is directly related to the NTR activity. A closer inspection of this process showed that the fluorescence of **hTf-PyTAP-NO$_2$** was gradually enhanced with increasing concentration of NTR (Fig. 3B) and is characterized by an exponential rather than linear increase. It can be explained by the fact that the bioconjugate can accommodate about eight molecules of dye which are not equally accessible to the enzyme. Thus, to convert dyes with lower accessibility, a higher enzyme concentration is needed, and this is manifested by an enhanced fluorescent signal observed for a higher enzyme concentration. However, due to the relatively high fluorescence of the **hTf-PyTAP-NO$_2$** bioconjugate and insufficient signal enhancement after reduction, it cannot be used exclusively for NTR quantification in a complex system/environment.

Simultaneously with the increase in fluorescence, a disappearance of the band at 340 nm in the absorption spectrum, characteristic for NADH is observed (Fig. 4A). This clearly indicates that the reduction of nitro-aromatic group in the conjugated nitro-pyrazinotriazapentalene moieties is taking place. Therefore, the probe conjugated to hTf preserves its affinity to the enzyme. Time-dependent absorption spectra showed that the reduction proceeded in several steps (Fig. 4B), and analogous pattern was observed for similar probe based on nitro-pyrazinotriazapentalene scaffold in our previous studies [33]. The first step of the reaction was fast up to a few minutes under applied experimental conditions. The initial step was followed by a slower step (completed within ca. 2 h), which corresponds to the gradual depletion of NADH. The subsequent step was quite fast (completed within minutes), and resulted in a pronounced increase in the absorption, registered in the visible part of the spectra. The last stage of the process was particularly slow, as it was not completed even after 6 h. The observed changes suggest that several products are produced upon reduction catalyzed by NTR.

Based on our previous findings [33], we propose that the first step of the reduction, is the formation of nitroso derivatives, which can be further reduced to their hydroxylamine counterparts. Hydroxylamines are unstable compounds and can easily be re-oxidized to a nitroso derivative by molecular oxygen. The reduction of the formed nitro derivatives by NADH, which is used in the reaction in a more than 10-fold excess over the nitro groups present in **hTf-PyTAP-NO$_2$** bioconjugate, continues until the complete depletion of NADH. Identification of the final reduced products for **hTf-PyTAP-NO$_2$** bioconjugate was not possible due to the high complexity of this system. However, for a probe similar to that not conjugated to protein, the nitroso derivative and the azoxy dimer were predominant products [33]. The suggested mechanism relies solely on UV-Vis spectral changes analysis.

3.3. Response of hTf-PyTAP-NO$_2$ bioconjugate to type II nitroreductases

To study the response of **hTf-PyTAP-NO$_2$** to type II oxygen-sensitive NTRs, liver microsomes were used. These contain, among others, cytochrome P450 reductases that have nitroreductases activity [32]. Bioconjugate reduction in the presence of microsomes was carried out for 4 or 24 h at 37 °C under air-equilibrated conditions and at very low oxygen concentration (<1 ppm of pO$_2$ in a glovebox). The **hTf-PyTAP-NO$_2$**
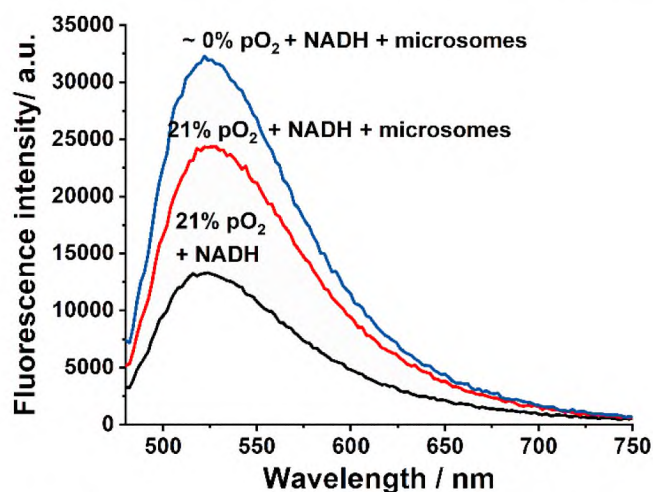

Fig. 5. The emission spectra (λ_{ext} 450 nm) of **hTf-PyTAP-NO$_2$** incubated with NADH (1 mM) without or with microsomes (1 mg/mL) after 4 h reaction undergoing under normoxic (21 % pO$_2$) or anaerobic conditions (< 1 ppm of pO$_2$, denoted as ~0 % pO$_2$). Experimental conditions: 50 mM TRIS-HCl buffer pH 7.4, 37 °C.

was reduced by the nitroreductases present in microsomes, as was demonstrated by an increase in the fluorescence emission, and as expected, the observed increase was more pronounced under oxygen depletion conditions (Fig. 5).

Separation of the reduction products employing size exclusion chromatography (SEC) revealed that in addition to the peak assigned to the protein fraction, peaks of low-molecular-weight products appeared (Fig. S2). When the reaction was carried out in the presence of microsomes, the amount of low-molecular-weight products was a small fraction. In the case of applying NTR from *E. Coli*, it was more pronounced, and its amount was linearly dependent on the applied enzyme concentration (Fig. S3mm). These observations suggest that upon reduction of the dye conjugated to transferrin catalyzed by NTRs, secondary
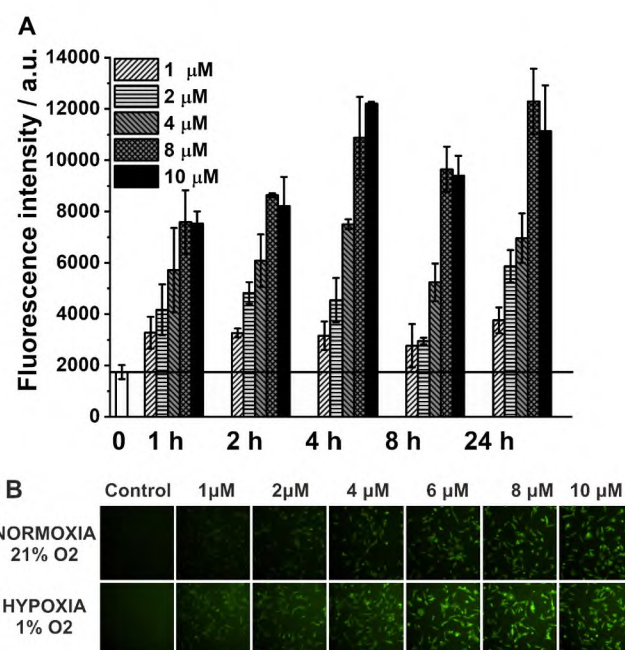

Fig. 6. (A) Fluorescence intensity of A2058 cells incubated with **hTf-PyTAP-NO$_2$** for different periods of time under normoxia ($\lambda_{ex/em}$ 450/530 nm). 0 denotes the blank sample; (B) Fluorescence images of A2058 cells incubated with **hTf-PyTAP-NO$_2$** for 4 h under normoxic and hypoxic conditions.
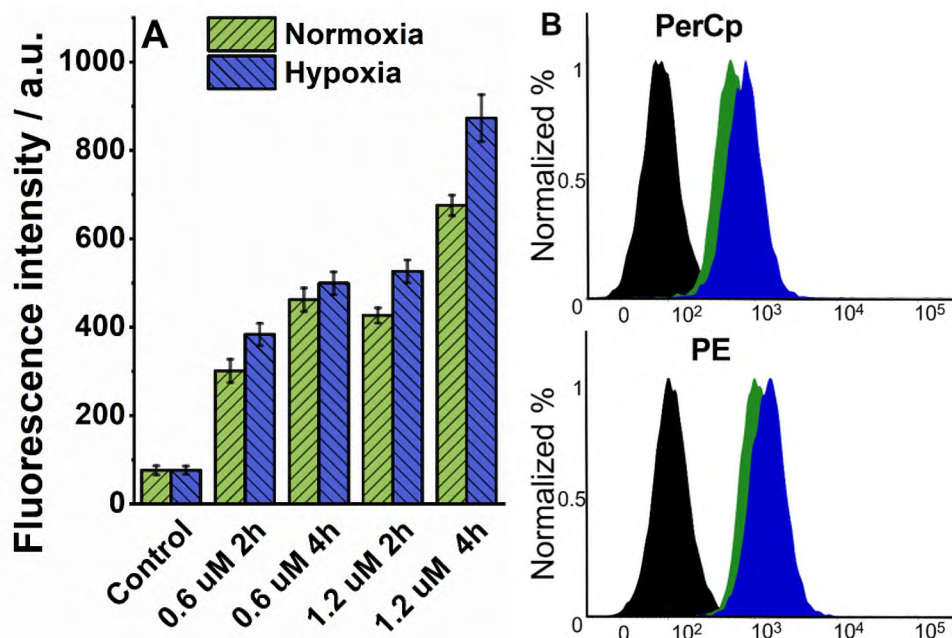
Fig. 7. (**A**) Fluorescence intensity **hTf-PyTAP-NO$_2$** incubated for 2 h or 4 h with A2058 cells under hypoxia (pO$_2$ 1 %) compared to cells kept under normoxia determined using flow cytometry (FITC 488/527 $\pm$ 16 nm). (**B**) Representative flow cytometry histograms measured at PerCP (488/700 $\pm$ 27 nm) and PE (488/586 $\pm$ 21 nm).

processes take place, leading to partial release of dye from the protein. In the presence of microsomes, the reductant products are scavenged by proteins present in the microsome homogenate. It is very likely that similar behavior is taking place in the cellular microenvironment allowing efficient trapping of dye inside cells, and this issue is discussed in the following Chapter.

3.4. In vitro cytotoxicity, photocytotoxicity, bioconjugate uptake and cell imaging

The highly metastatic human melanoma cell line A2058 was selected to evaluate the imaging properties of the **hTf-PyTAP-NO$_2$** bioconjugate in vitro. It was shown that A2058 cells express nitroreductases, which is enhanced under hypoxia conditions [33]. Therefore, increased emission from bioconjugate is expected in cells cultured under hypoxia as determined in model studies on microsomes (Fig. 5). To verify this hypothesis, A2058 cells were cultured under normoxic and hypoxic conditions. To obtain the population of cells exposed to hypoxia, they were cultured in a hypoxic chamber (1 % pO$_2$) 24 h before the experiment. The use of sensors in vitro requires non-toxic doses of compounds. The bioconjugate and the free dye showed neither cytotoxic nor photocytotoxic activity in the concentration range and light doses applied in imaging experiments (Figs. S4 and S5).

The time and concentration-dependent accumulation of the **hTf-PyTAP-NO$_2$** bioconjugate in A2058 cells is shown in Fig. 6. The tested bioconjugate accumulates in cells very quickly even at low concentrations, reaching a fluorescence maximum after only 2–4 h (Fig. 6A). In addition, no decrease in fluorescence level was observed within one day, which makes the sensor extremely stable in cells. For further experiments, 2 and 4 h were chosen as the optimal accumulation time for the **hTf-PyTAP-NO$_2$** bioconjugate. As shown in Fig. 6B, the fluorescence images of A2058 cells show a dose-dependent increase in cell fluorescence, more pronounced for cells cultured under hypoxic conditions.

To quantify fluorescence intensity from A2058 cells cultured under normoxia and hypoxia and incubated with **hTf-PyTAP-NO$_2$** bioconjugate for 2 or 4 h, they were analyzed using a flow cytometer. The obtained data (Fig. 7) show a clear difference between the
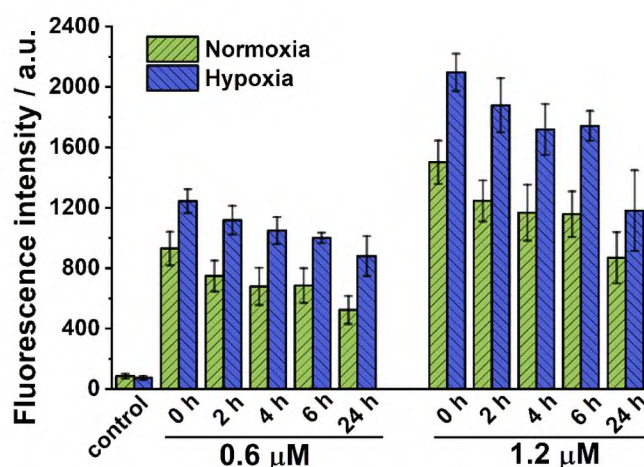

Fig. 8. Fluorescence intensity of A2058 cells treated with **hTf-PyTAP-NO$_2$** (0.6 μM or 1.2 μM) for 4 h under normoxic (pO$_2$ 21 %) or hypoxic (pO$_2$ 1 %) conditions at different times intervals after sensor removal of the sensor. Data was obtained using flow cytometry (FITC 488/527 $\pm$ 16 nm).

autofluorescence of control cells and those stained with bioconjugate. The difference was registered at different channels FITC (488/527 $\pm$ 16 nm), PE (488/586 $\pm$ 21 nm), and PerCP (488/700 $\pm$ 27 nm), which makes this sensor quite universal in terms of optical devices. A low concentration of bioconjugate (0.6 μM) and a short incubation time with cells were enough to obtain a good signal and easily differentiate treated cells from untreated ones. For both studied concentrations and incubation times, the fluorescence intensity of cells incubated with bioconjugate slightly increased under hypoxic conditions however the difference between the fluorescence signals is too small to indicate the oxygenation state of cells. The small increase in fluorescent signal can be associated with a more effective reduction of the nitro group in the probe due to elevated level of nitroreductases.
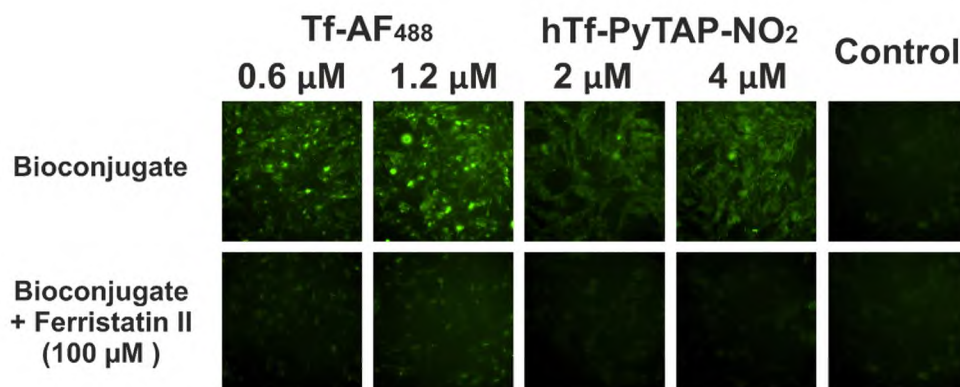
Fig. 9. Fluorescence images of untreated A2058 cells (control) or after 4 h of incubation with Tf-AF$_{488}$ or **hTf-PyTAP-NO$_2$** bioconjugates alone or together with ferristatin II (100 μM) preincubated 24 h before applying Tf bioconjugates. Experiment was performed under normoxic (pO$_2$ 21 %) conditions.

3.5. Sensor retention in cells

Sensor retention in cells and its resistance to degradation in the cellular environment are two key parameters that need to be considered for in vivo application. To verify the efficiency in cell staining, the bioconjugate was incubated for 4 h with cells, then the unaccumulated sensor was washed out, and the intensity of the fluorescence of cells was monitored for up to 24 h. As shown in Fig. 8, during the first 2 h, the level of cell fluorescence decreases by 20 % at normoxia and only 10 % at hypoxia. The recycling of the internalized transferrin via the transferrin receptor back to the extracellular cell surface in a cancer cell occurs quickly, within a few minutes.[13].

Closer inspection of the supernatant collected from cells revealed that the amount of bioconjugate was much less than 1 % of the applied dose, while the total concentration of transferrin did not exceed 10 % (Fig. S6). The emission from low-molecular-weight derivatives of the probe found in the supernatant also remained at a very low level suggesting that the efflux of the free probe was not efficient (Fig. S6). These observations suggest that the bioconjugate is entrapped in cells and only partially the sensor is released from it in the cell. Furthermore, the free probe might also resist efflux due to the interaction with proteins as suggested for probes possessing nitroaromatic unit [48]. Fluorescent emission from cells after 24 h of staining remained quite high, showing a decrease of less than 55 %. The emission of cells cultured under hypoxia was higher in all checked time intervals, and its decrease was more sluggish than at normoxia.

3.6. TfR-mediated delivery of bioconjugate

To confirm the internalization of the **hTf-PyTAP-NO$_2$** bioconjugate through the transferrin receptor pathway, ferristatin II (NSC8679) – a TfR1 inhibitor, was used to inhibit transferrin uptake. Ferristatin II, by degrading the TfR1 prevents Tf uptake by the cell [49,50]. Initial studies were performed using a commercial Tf-AlexaFluor488 bioconjugate (Tf-AF$_{488}$). A dose-dependent inhibition of Tf-AF$_{488}$ uptake was observed when cells were pretreated with ferristatin II for 24 h (Fig. S7). The IC$_{50}$ value for receptor inhibition was 54.2 ± 7.8 μM. For experiments with the synthesized **hTf-PyTAP-NO$_2$** bioconjugate, a 100 μM concentration of ferristatin II was used. As shown in Fig. 9, the addition of the inhibitor completely blocked the uptake of the **hTf-PyTAP-NO$_2$** bioconjugate and Tf-AF$_{488}$, as demonstrated by the decrease in fluorescence exhibited by cells treated with these compounds. It confirms that the uptake of the bioconjugate occurring by endocytosis is the only cellular transport mechanism.

Furthermore, to evaluate the affinity of the **hTf-PyTAP-NO$_2$** bioconjugate to TfR, a competitive experiment was designed. Uptake of **hTf-PyTAP-NO$_2$** by A2058 cells was evaluated in the presence of a 10-fold excess of unmodified hTf over bioconjugate and compared to the
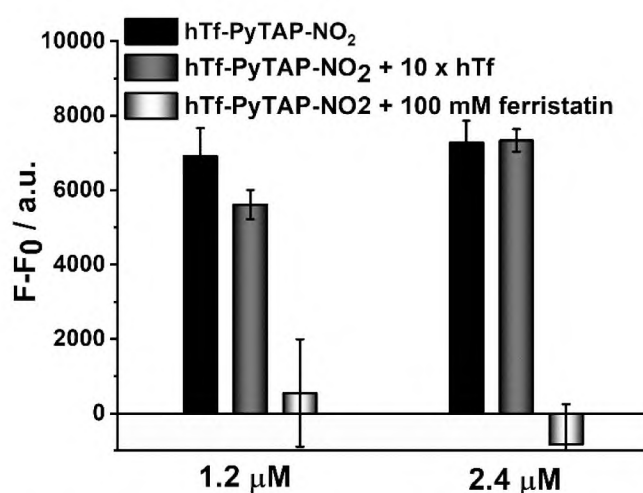

Fig. 10. Changes in the fluorescence of A2058 cells after 1 h incubation with **hTf-PyTAP-NO$_2$** bioconjugate alone, in the presence of 10-fold excess holo-transferrin (hTf) or 100 μM of ferristatin II preincubated with cells 24 h prior addition of bioconjugate Untreated cells were used as a control. Experiment was performed under normoxic (pO$_2$ 21 %) conditions using plate reader ($\lambda_{ex/em}$ 450/530 nm).

uptake of bioconjugate administered alone. As a negative control, cells pre-treated with ferristatin II were used. The excess of unmodified hTf has been shown not to adversely affect the uptake efficiency of the hTf bioconjugate (Fig. 10). This suggests that the resulting **hTf-PyTAP-NO$_2$** bioconjugate may have an even higher affinity for the TfR than hTf itself. Such an effect was not observed for commercially available Tf-AF$_{488}$ (Fig. S8).

4. Conclusions

We propose a new sensor for imaging cancer cells, whose selectivity is based on its exclusive uptake via transferrin receptor endocytosis. Bioconjugation of holo-transferrin with a nitro-pyrazinotriazapentalene scaffold as a fluorophore precursor resulted in a sensor characterized by fast and efficient uptake and sustained intracellular retention. The accommodation of eight molecules of the fluorophore within the protein allows achieving a higher fluorescent signal, which is additionally amplified under hypoxic conditions, increasing the reduction of the nitro group because of the overexpression of nitroreductases. Furthermore, only small decrease in the fluorescence signal is observed within one day, which makes the sensor exceptionally stable in the cell. The proposed sensor offers a practical tool for detecting cells expressing

transferrin receptors through fluorescence microscopy imaging, flow cytometry, or even a simple microplate reader and for cell differentiation based on nitroreductase activity. It also has the potential to be applied as a sensor for intraoperative tumor-specific fluorescence imaging in vivo or for semi-quantitative *ex vivo* analyses.

CRediT authorship contribution statement

Ewelina Janczy-Cempa investigation, methodology, visualization, formal analysis, writing – original draft for bioconjugate formation, characterization, NTRs and in vitro studies. **Olga Mazuryk** investigation, validation, supervision for in vitro studies. **Anna Kwiatkowska** investigation organic synthesis. **Nicolas Chopin** investigation, formal analysis for organic synthesis, **Marie-Aude Hiebel** formal analysis, supervision, writing – original draft for organic synthesis. **Franck Suzenet** conceptualization, supervision, funding acquisition, writing – original draft. **Małgorzata Brindell** conceptualization, supervision, funding acquisition, writing – original draft, writing – review & editing.

Declaration of Competing Interest

The authors declare that they have no known competing financial interests or personal relationships that could have appeared to influence the work reported in this paper.

Data Availability

Data will be made available on request.

Acknowledgements

Appendix A. Supporting information

Supplementary data associated with this article can be found in the online version at doi:10.1016/j.snb.2023.134450.

References

[1] L. Fass, Imaging and cancer: a review, Mol. Oncol. 2 (2008) 115–152, https://doi.org/10.1016/j.molonc.2008.04.001.
[2] L.J. Lauwerends, P.B.A.A. Van Driel, R.J. Baatenburg de Jong, J.A.U. Hardillo, S. Koljenovic, G. Puppels, L. Mezzanotte, C.W.G.M. Löwik, E.L. Rosenthal, A.L. Vahrmeijer, S. Keereweer, Real-time fluorescence imaging in intraoperative decision making for cancer surgery, Lancet Oncol. 22 (2021) 186–195, https://doi.org/10.1016/S1470-2045(20)30600-8.
[3] S. Keereweer, P.B.A.A. Van Driel, T.J.A. Snoeks, J.D.F. Kerrebijn, R.J.B. De Jong, A.L. Vahrmeijer, H.J.C.M. Sterenborg, C.W.G.M. Löwik, Optical image-guided cancer surgery: challenges and limitations, Clin. Cancer Res 19 (2013) 3745–3754, https://doi.org/10.1158/1078-0432.CCR-12-3598.
[4] D. Hanahan, Hallmarks of cancer: new dimensions, Cancer Discov. 12 (2022) 31–46, https://doi.org/10.1158/2159-8290.CD-21-1059.
[5] Z. Hu, R. Li, X. Cui, C. Hu, Z. Chen, A pH-sensitive carbonic anhydrase IX-targeted near-infrared probe for fluorescent sensing and imaging of hypoxic osteosarcoma, Sens Actuators B Chem. 379 (2023), 133171, https://doi.org/10.1016/J.SNB.2022.133171.
[6] G.M. Van Dam, G. Themelis, L.M.A. Crane, N.J. Harlaar, R.G. Pleijhuis, W. Kelder, A. Sarantopoulos, J.S. De Jong, H.J.G. Arts, A.G.J. Van Der Zee, J. Bart, P.S. Low, V. Ntziachristos, Intraoperative tumor-specific fluorescence imaging in ovarian cancer by folate receptor-α targeting: first in-human results, Nat. Med 17 (2011) 1315–1319, https://doi.org/10.1038/NM.2472.

[7] M. Koller, S.Q. Qiu, M.D. Linssen, L. Jansen, W. Kelder, J. de Vries, I. Kruithof, G.J. Zhang, D.J. Robinson, W.B. Nagengast, A. Jorritsma-Smit, B. van der Vegt, G.M. Van Dam, Implementation and benchmarking of a novel analytical framework to clinically evaluate tumor-specific fluorescent tracers, Nat. Commun. 9 (1) (2018) 11, https://doi.org/10.1038/s41467-018-05727-y.
[8] N.J. Harlaar, M. Koller, S.J. de Jongh, B.L. van Leeuwen, P.H. Hemmer, S. Kruijff, R.J. van Ginkel, L.B. Been, J.S. de Jong, G. Kats-Ugurlu, M.D. Linssen, A. Jorritsma-Smit, M. van Oosten, W.B. Nagengast, V. Ntziachristos, G.M. van Dam, Molecular fluorescence-guided surgery of peritoneal carcinomatosis of colorectal origin: a single-centre feasibility study, Lancet Gastroenterol. Hepatol. 1 (2016) 283–290, https://doi.org/10.1016/S2468-1253(16)30082-6.
[9] P. Aisen, A. Leibman, J. Zweier, Stoichiometric and site characteristics of the binding of iron to human transferrin, J. Biol. Chem. 253 (1978) 1930–1937, https://doi.org/10.1016/S0021-9258(19)62337-9.
[10] Y. Shen, X. Li, D. Dong, B. Zhang, Y. Xue, P. Shang, Transferrin receptor 1 in cancer: a new sight for cancer therapy, Am. J. Cancer Res 8 (2018) 916. /pmc/articles/PMC6048407/ (accessed August 30, 2022).
[11] P.V. Candelaria, L.S. Leoh, M.L. Penichet, T.R. Daniels-Wells, Antibodies targeting the transferrin receptor 1 (TfR1) as direct anti-cancer agents, Front Immunol. 12 (2021) 583, https://doi.org/10.3389/fimmu.2021.607692.
[12] S. Sarkar, H. Lee, H.G. Ryu, S. Singha, Y.M. Lee, Y.J. Reo, Y.W. Jun, K.H. Kim, W.J. Kim, K.H. Ahn, A study on hypoxia susceptibility of organ tissues by fluorescence imaging with a ratiometric nitroreductase probe, ACS Sens 6 (2021) 148–155, https://doi.org/10.1021/acssensors.0c01989.
[13] S. Tortorella, T.C. Karagiannis, S. Tortorella, T.C. Karagiannis, Transferrin receptor-mediated endocytosis: a useful target for cancer therapy, J. Membr. Biol. 247 (2014) 291–307, https://doi.org/10.1007/S00232-014-9637-0.
[14] D.R. Richardson, P. Ponka, The molecular mechanisms of the metabolism and transport of iron in normal and neoplastic cells, Biochim Biophys. Acta 1331 (1997) 1–40, https://doi.org/10.1016/S0304-4157(96)00014-7.
[15] J. Wang, S. Tian, R.A. Petros, M.E. Napier, J.M. Desimone, The complex role of multivalency in nanoparticles targeting the transferrin receptor for cancer therapies, J. Am. Chem. Soc. 132 (2010) 11306–11313, https://doi.org/10.1021/ja1043177.
[16] D. Abegg, G. Gasparini, D.G. Hoch, A. Shuster, E. Bartolami, S. Matile, A. Adibekian, Strained cyclic disulfides enable cellular uptake by reacting with the transferrin receptor, J. Am. Chem. Soc. 139 (2017) 231–238, https://doi.org/10.1021/jacs.6b09643.
[17] T.R. Daniels, E. Bernabeu, J.A. Rodríguez, S. Patel, M. Kozman, D.A. Chiappetta, E. Holler, J.Y. Ljubimova, G. Helguera, M.L. Penichet, The transferrin receptor and the targeted delivery of therapeutic agents against cancer, Biochim Biophys. Acta 1820 (2012) 291–317, https://doi.org/10.1016/j.bbagen.2011.07.016.
[18] Q. Sha, B. Sun, C. Yi, R. Guan, J. Fei, Z. Hu, B. Liu, X. Liu, A fluorescence turn-on biosensor based on transferrin encapsulated gold nanoclusters for 5-hydroxytryptamine detection, Sens Actuators B Chem. 294 (2019) 177–184, https://doi.org/10.1016/J.SNB.2019.05.060.
[19] Y. Li, L. Zhao, X.F. Li, Targeting hypoxia: hypoxia-activated prodrugs in cancer therapy, Front Oncol. 11 (2021) 2920, https://doi.org/10.3389/fonc.2021.700407.
[20] V. Petrova, M. Annicchiarico-Petruzzelli, G. Melino, I. Amelio, The hypoxic tumour microenvironment, Oncogenesis 7 (1) (2018) 13, https://doi.org/10.1038/s41389-017-0011-9.
[21] G.L. Semenza, Hypoxia-inducible factors in physiology and medicine, Cell 148 (2012) 399–408, https://doi.org/10.1016/j.cell.2012.01.021.
[22] P.H. Maxwell, The HIF pathway in cancer, Semin Cell Dev. Biol. 16 (2005) 523–530, https://doi.org/10.1016/j.semcdb.2005.03.001.
[23] J.C. Walsh, A. Lebedev, E. Aten, K. Madsen, L. Marciano, H.C. Kolb, The clinical importance of assessing tumor hypoxia: relationship of tumor hypoxia to prognosis and therapeutic opportunities, Antioxid. Redox Signal 21 (2014) 1516–1554, https://doi.org/10.1089/ars.2013.5378.
[24] S.A. Anderson, C.P. Nizzi, Y.I. Chang, K.M. Deck, P.J. Schmidt, B. Galy, A. Damnernsawad, A.T. Broman, C. Kendziorski, M.W. Hentze, M.D. Fleming, J. Zhang, R.S. Eisenstein, The IRP1-HIF-2α axis coordinates iron and oxygen sensing with erythropoiesis and iron absorption, Cell Metab. 17 (2013) 282–290, https://doi.org/10.1016/j.cmet.2013.01.007.
[25] W.W. Wheaton, N.S. Chandel, Hypoxia. 2. Hypoxia regulates cellular metabolism, Am. J. Physiol. Cell Physiol. 300 (2011), https://doi.org/10.1152/ajpcell.00485.2010.
[26] L.S. Ryan, J. Gerberich, J. Cao, W. An, B.A. Jenkins, R.P. Mason, A.R. Lippert, Kinetics-based measurement of hypoxia in living cells and animals using an acetoxymethyl ester chemiluminescent probe, ACS Sens 4 (2019) 1391–1398, https://doi.org/10.1021/acssensors.9b00360.
[27] Q. Lin, C. Li, L. Wang, H. Cai, L. Tang, Y. Gu, Ultrasensitive near-infrared fluorescence probe activated by nitroreductase for in vivo hypoxia detection, Sens Actuators B Chem. 371 (2022), 132521, https://doi.org/10.1016/J.SNB.2022.132521.
[28] C.A. Haynes, R.L. Koder, A.F. Miller, D.W. Rodgers, Structures of nitroreductase in three states: effects of inhibitor binding and reduction, J. Biol. Chem. 277 (2002) 11513–11520, https://doi.org/10.1074/jbc.M111334200.
[29] J.L. Klockow, K.S. Hettie, E.L. LaGory, E.J. Moon, A.J. Giaccia, E.E. Graves, F.T. Chin, An activatable NIR fluorescent rosol for selectively imaging nitroreductase activity, Sens Actuators B Chem. 306 (2020), 127446, https://doi.org/10.1016/J.SNB.2019.127446.
[30] K. Zhu, T. Qin, C. Zhao, Z. Luo, Y. Huang, B. Liu, L. Wang, A novel fluorescent turn-on probe for highly selective detection of nitroreductase in tumor cells, Sens

Actuators B Chem. 276 (2018) 397–403, https://doi.org/10.1016/j.snb.2018.08.134.

[31] J. Qiao, M. Wang, M. Cui, Y. Fang, H. Li, C. Zheng, Z. Li, Y. Xu, H. Hua, D. Li, Small-molecule probes for fluorescent detection of cellular hypoxia-related nitroreductase, J. Pharm. Biomed. Anal. 203 (2021), https://doi.org/10.1016/j.jpba.2021.114199.

[32] E. Janczy-Cempa, O. Mazuryk, A. Kania, M. Brindell, Significance of specific oxidoreductases in the design of hypoxia-activated prodrugs and fluorescent turn off-on probes for hypoxia imaging, Cancers (Basel) 14 (2022) 2686, https://doi.org/10.3390/cancers14112686.

[33] E. Janczy-Cempa, O. Mazuryk, D. Sirbu, N. Chopin, M. Zarnik, M. Zastawna, C. Colas, M.-A. Hiebel, F. Suzenet, M. Brindell, Nitro-pyrazinotriazapentalene scaffolds-nitroreductase quantification and in vitro fluorescence imaging of hypoxia, Sens Actuators B Chem. 346 (2021) 925–4005, https://doi.org/10.1016/j.snb.2021.130504.

[34] J.V. Jun, D.M. Chenoweth, E.J. Petersson, Rational design of small molecule fluorescent probes for biological applications, Org. Biomol. Chem. 18 (2020) 5747, https://doi.org/10.1039/D0OB01131B.

[35] Y. Lu, H. Liao, T. Li, W. Sun, J. Liang, Y.Q. Zhao, H. Zhao, Y. Zhou, Optical monitoring and treatment of breast cancer by a tumor hypoxia-activated multi-functional fluorescent sensor, Sens Actuators B Chem. 377 (2023), https://doi.org/10.1016/J.SNB.2022.133030.

[36] F. Xue, C. Li, Y. Kuang, L. Shi, J. Chen, S.X. Chen, M. Ma, X. Wang, H. Chen, A NTR and O2 programmed responsive photogenic radicals for efficient hypoxia cancer therapy, Sens Actuators B Chem. 369 (2022), https://doi.org/10.1016/J.SNB.2022.132311.

[37] J.N. Liu, W. Bu, J. Shi, Chemical design and synthesis of functionalized probes for imaging and treating tumor hypoxia, Chem. Rev. 117 (2017) 6160–6224, https://doi.org/10.1021/acs.chemrev.6b00525.

[38] Y.L. Qi, L. Guo, L.L. Chen, H. Li, Y.S. Yang, A.Q. Jiang, H.L. Zhu, Recent progress in the design principles, sensing mechanisms, and applications of small-molecule probes for nitroreductases, Coord. Chem. Rev. 421 (2020), 213460, https://doi.org/10.1016/j.ccr.2020.213460.

[39] S. Sandhu, L. Kydd, J. Jaworski, Luminescent probe based techniques for hypoxia imaging, J. Nanomed. Res 6 (2017), https://doi.org/10.15406/jnmr.2017.06.00160.

[40] S. Luo, R. Zou, J. Wu, M.P. Landry, A probe for the detection of hypoxic cancer cells, ACS Sens 2 (2017) 1139–1145, https://doi.org/10.1021/acssensors.7b00171.

[41] Y. Zhang, X.F. Zhang, Q. Chen, X.Q. Cao, S.L. Shen, A novel near-infrared fluorescence off-on probe for imaging hypoxia and nitroreductase in cells and in vivo, Sens Actuators B Chem. 353 (2022) 131–145, https://doi.org/10.1016/J.SNB.2021.131145.

[42] J. Xue, Y. Liu, L. Li, J. Xu, T. Chen, Y. Li, G. Chen, Visualizing the hypoxic heterogeneity for distinguishing the cancer tissues with a two-photon nitroreductase-H2S logic probe via intramolecular isomerization, Sens Actuators B Chem. 347 (2021), 130647, https://doi.org/10.1016/J.SNB.2021.130647.

[43] W. Du, J. Wang, H. Fang, W. Ji, Y. Liu, Y. Qu, D. Zhang, T. Shao, X. Hou, Q. Wu, L. Li, Mitochondria-specific two-photon fluorogenic probe for simultaneously visualizing nitroreductase and viscosity in cancer cells, Sens Actuators B Chem. 370 (2022), 132456, https://doi.org/10.1016/J.SNB.2022.132456.

[44] M. Daniel, M.A. Hiebel, G. Guillaumet, E. Pasquinet, F. Suzenet, Intramolecular metal-free N–N bond formation with heteroaromatic amines: mild access to fused-triazapentalene derivatives, Chem. - Eur. J. 26 (2020) 1525–1529, https://doi.org/10.1002/chem.201905558.

[45] D. Sirbu, J. Diharce, I. Martinić, N. Chopin, S.V. Eliseeva, G. Guillaumet, S. Petoud, P. Bonnet, F. Suzenet, An original class of small sized molecules as versatile

fluorescent probes for cellular imaging, Commun. Chem. 55 (2019) 7776–7779, https://doi.org/10.1039/C9CC03765A.

[46] D. Sirbu, N. Chopin, I. Martinić, M. Ndiaye, S.V. Eliseeva, M.A. Hiebel, S. Petoud, F. Suzenet, Pyridazino-1,3a,6a-triazapentalenes as versatile fluorescent probes: impact of their post-functionalization and application for cellular imaging, Int J. Mol. Sci. 22 (2021) 6645, https://doi.org/10.3390/ijms22126645.

[47] C. Nyffenegger, E. Pasquinet, F. Suzenet, D. Poullain, C. Jarry, J.-M. Léger, G. Guillaumet, An efficient route to polynitrogen-fused tricycles via a nitrene-mediated N–N bond formation under microwave irradiation, Tetrahedron 64 (2008) 9567–9573, https://doi.org/10.1016/j.tet.2008.07.055.

[48] S. Kizaka-Kondoh, H. Konse-Nagasawa, Significance of nitroimidazole compounds and hypoxia-inducible factor-1 for imaging tumor hypoxia, Cancer Sci. 100 (2009) 1366–1373, https://doi.org/10.1111/j.1349-7006.2009.01195.x.

[49] L. Horonchik, M. Wessling-Resnick, The small-molecule iron transport inhibitor ferristatin/NSC306711 promotes degradation of the transferrin receptor, Chem. Biol. 15 (2008) 647, https://doi.org/10.1016/j.chembiol.2008.05.011.

[50] S.L. Byrne, P.D. Buckett, J. Kim, F. Luo, J. Sanford, J. Chen, C. Enns, M. Wessling-Resnick, Ferristatin II promotes degradation of transferrin receptor-1 in vitro and in vivo, PLoS One 8 (2013), https://doi.org/10.1371/journal.pone.0070199.

Ewelina Janczy-Cempa obtained her MSc Degree in Chemistry in 2018 from the Jagiellonian University. She is currently Ph.D. student at the same University. Her scientific interest is mainly devoted to designing sensor for hypoxia assessment.

Anna Kwiatkowska obtained her MSc Degree in Chemistry in 2019 from the Jagiellonian University. She is now working for a chemical company dedicated to the development of various bioactive compounds.

Olga Mazuryk obtained her Doctoral degree in 2015 from the Jagiellonian University. Currently she is an Assistant Professor of Faculty of Chemistry of the Jagiellonian University. Her research efforts are focused on anticancer effects of metal-based compounds, their bioactivity in hypoxic conditions, and improved delivery.

Nicolas Chopin obtained his Doctor Degree in chemistry from Lyon University in 2012. After specialization in fluorescence and therapeutic chemistry, his research interests are drugs and luminescent probes syntheses. He is now working for a chemical company dedicated to the development of various bioactive compounds.

Marie-Aude Hiebel obtained her Doctor Degree in organic chemistry from Claude Bernard Lyon 1 University in 2008. Now she is an assistant Professor in Institut de Chimie Organique et Analytique (Orléans University, France) major in organic chemistry. Her current research interests are heterocyclic and medicinal chemistry.

Franck Suzenet obtained his Doctor Degree in chemistry from University of Nantes in 1998. He was appointed at the University of Orleans in 2000 and got a full professor position at the same University in 2014. His research interests are heteroaromatic chemistry for medicinal chemistry and fluorescent probe developments.

Małgorzata Brindell received her Doctoral degree in 2004 from the Jagiellonian University. Since 2018 she has been Professor of the Jagiellonian University and is the Head of the Education Program in Medicinal Chemistry. Her research activities cover many aspects of bioinorganic and medicinal chemistry, among others the application of metal compounds in the treatment and diagnosis of cancer and designing of optical sensors for assessment of hypoxia in tissue.